Soft Matter

PAPER

View Article Online
View Journal | View Issue

Cite this: *Soft Matter*, 2015, 11, 8701

Lateral capillary interactions between colloids beneath an oil–water interface that are driven by out-of-plane electrostatic double-layer interactions†

Bum Jun Park,*[a] Mina Lee,[a] Bomsock Lee[a] and Eric M. Furst[b]

Received 11th August 2015,
Accepted 9th September 2015

DOI: 10.1039/c5sm02001h

www.rsc.org/softmatter

We study the lateral capillary interactions between colloids beneath an oil–water interface that lead to closely packed two-dimensional self-assembled colloidal crystals. These capillary forces are caused by the overlap of deformed interfaces above colloids on a solid substrate. The interface deformation is due to the electrostatic disjoining pressure between the charged particles and the charged oil–water interface. It is notable that the short-range (*i.e.*, on the nanometer scale) and out-of-plane electrostatic double-layer interactions, which occur through an aqueous phase, can generate the long-range lateral capillary attraction (*i.e.*, on the micrometer scale).

Introduction

The microstructure and stability of colloidal dispersions are determined by several factors, such as the volume fraction of particles, concentration of additives (*i.e.*, electrolytes, surfactants, and polymers), temperature, and the dielectric constant of the fluid medium.[1–6] In particular, when colloids are confined at a two-dimensional (2D) fluid–fluid interface, where one phase is an electrolyte medium and the other carries relatively few charges (*i.e.*, air–water or oil–water interfaces), they interact on a long-range $O(1)$–$O(2)$ micrometer scale.[7–9] This interaction is attributed to two interparticle interaction forces: electrostatic interactions[10–16] and capillary interactions.[13,17–19] By controlling such interaction forces, the colloidal microstructure and mechanical/rheological behaviors can be manipulated.[12,20–23]

Interactions between dissimilar surfaces (*e.g.*, colloids and fluid interfaces) are also a significant factor for stabilizing a variety of immiscible fluids, such as Pickering emulsions, colloidosomes, bijel (bicontinuous, interfacially-jammed emulsion gel), and colloid-stabilized polymer blends.[24–27] Notably, prior to the strong attachment of colloidal particles to a fluid–fluid interface (*e.g.*, an attachment energy of $\Delta E_{att} \sim -10^8 k_B T$),[28] the electrostatic repulsion between the particles and the fluid interface imparts a threshold energy against attachment.[29–31] These interactions (*i.e.*, the disjoining pressure) between a charged particle and a charged fluid interface can be measured using a surface force apparatus (SFA) and calculated by solving the Poisson–Boltzmann (PB) equation.[29–31]

Such electrostatic interactions between dissimilar surfaces (*i.e.*, colloidal particles and oil–water interfaces), which are typically short-range (*i.e.*, nanometer scale), can generate a long-range capillary force that acts as the driving force for the assembly of particles that are captured between the interface and a solid substrate (*i.e.*, the fluid interface templating method).[32] As shown in Fig. 1, the height of an oil–water interface decreases *via* hydrostatic pressure. When the interface height is comparable to the particle size, the disjoining pressure between the particles and the oil–water interface likely deforms the interface above the particles. We believe that the overlap between adjacent interface deformations causes the lateral capillary interaction to minimize the surface free energy; consequently, this should act as the driving force for the closely packed two-dimensional self-assembly of particles beneath the oil–water interface (Fig. 1). This paper presents a detailed mechanism of this newly discovered type of capillary interaction.

Note that a similar assembly technique of colloidal particles was reported previously by Denkov *et al.*[33] They proposed that the driving force for assembly is induced convectively by the evaporation of water and the immersion capillary force produced as the particles protrude from the air–water interface. Based on the experimental observations in our system, however, the disjoining pressure between the particles and the oil–water interface hinders such protrusion.[32] Furthermore, we also observed that the closely packed particles underneath the oil–water interface eventually transfer to the interface and immediately exhibit long-range repulsions (*i.e.*, a dewetting transition),[32] which is a hallmark of colloidal interactions at an oil–water interface.[10–16] These observations suggest that assembly occurs beneath the oil–water interface. Therefore, the immersion capillary force is unlikely to account for the observed assembly behavior.[33]

[a] *Department of Chemical Engineering, Kyung Hee University, Yongin, 17104, South Korea. E-mail: bjpark@khu.ac.kr; Tel: +82-31-201-2429*
[b] *Department of Chemical and Biomolecular Engineering and Center for Molecular & Engineering Thermodynamics, University of Delaware, Newark, Delaware 19716, USA*

† Electronic supplementary information (ESI) available: The detailed method of the initial value problem, and Movies S1 and S2. See DOI: 10.1039/c5sm02001h

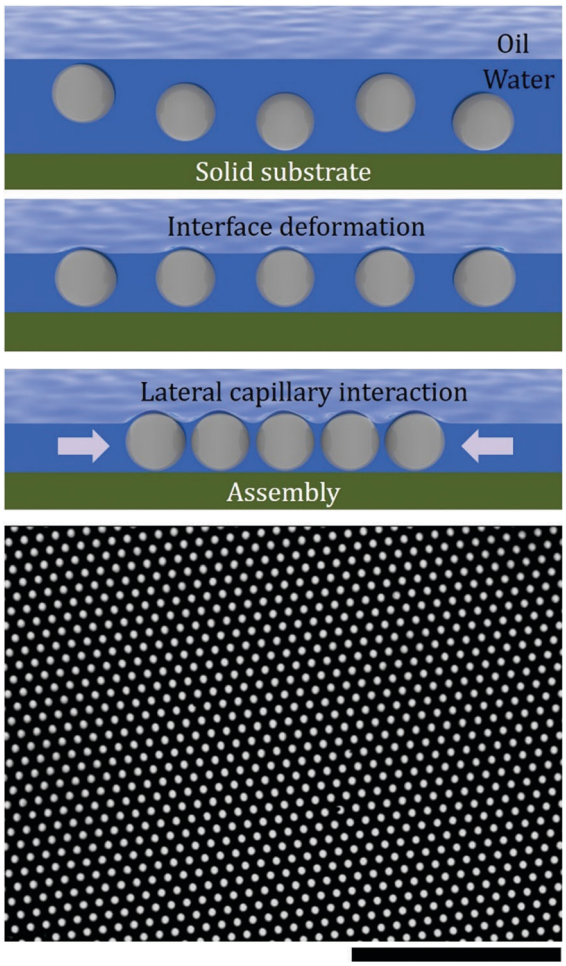

Fig. 1 Schematic of the self-assembled colloidal crystal *via* fluid interface templating. The bottom image is a snapshot of a 2D colloidal crystal extracted from Movie S1 in the ESI.† The scale bar is 30 μm.

In this paper, we examine the driving force of colloidal assembly beneath the oil–water interface *via* fluid interface templating.[32] This paper is organized as follows. First, we briefly describe the experimental procedure for particle assembly. Then, we calculate the electrostatic disjoining pressure between the charged particles and the charged oil–water interface. These results are compared to numerical solutions using the non-linear PB equation. To obtain the deformed interface profiles above the particles, we solve the augmented Young–Laplace (AYL) equation.[29,30,34,35] Based on the interface deformation, the free energy change and the corresponding lateral capillary attraction between particles are numerically calculated. Finally, we compare the calculated capillary force with the pair interaction forces, which are measured using optical laser tweezers.[2,14]

Materials and methods

Experimental

The experimental setup consists of a glass outer cylinder and an inner cylinder placed on an inverted microscope stage (Zeiss Axiovert 200).[14,32] The bottom of the outer cylinder is attached to a 40 mm circular glass coverslip (No. 1.5 Fisherbrand) using UV curing epoxy (Norland Products, NOA 81). The bottom of the inner cylinder, which is placed on the coverslip, is composed of aluminum and Teflon in order to pin the oil–water interface. Surfactant-free, charge-stabilized polystyrene particles with sulfate groups (Interfacial Dynamics Corp., σ = 6.2 μC cm^{-2} and $2a$ = 2.9 ± 0.12 μm in diameter) are initially suspended in the aqueous subphase (ultra-purified water, resistivity >18.2 MΩ cm). Subsequently, *n*-decane (Acros Organics, 99+%) is added to form the nonpolar superphase (Fig. 1). Note that *n*-decane has been filtered through aluminum oxide particles (Acros Chemical, acidic-activated, particle size 100–500 μm) to remove any polar contaminants. The entire cell is enclosed by another coverslip in order to minimize convection and water evaporation. We control the height of the interface *via* the hydrostatic pressure generated by adding or removing water from the outer cylinder. All glassware is cleaned using a plasma cleaner (Harrick Plasma, PDC 32-G) to achieve good wetting conditions for water. To measure interactions between two particles dispersed in the aqueous solution, we use time-sharing optical laser tweezers. For a detailed description of the laser tweezer apparatus, we refer the reader to our previously reported work.[2,14,32]

Disjoining pressure

The disjoining pressure is characterized by an analogue of the Derjaguin–Landau–Verwey–Overbeek (DLVO) interaction.[36] The van der Waals interaction between two parallel planes is non-dimensionalized by the surface tension γ and the inverse Debye screening length κ and is given by:

$$\hat{\Pi}_{\mathrm{vdW}} = \frac{\Pi_{\mathrm{vdW}}}{\gamma\kappa} = -\frac{A_{\mathrm{eff}}\kappa^2}{6\pi\gamma\hat{h}^3}.$$

Here, A_{eff} is the effective Hamaker constant of the two planes in a continuous medium, and $\hat{h} = \kappa h$ is the nondimensionalized surface-to-surface distance. The Debye screening length is given by:

$$\kappa^{-1} = \left[\frac{1000e^2 N_{\mathrm{A}} 2I}{\varepsilon_{\mathrm{W}}\varepsilon_0 k_{\mathrm{B}} T}\right]^{-1/2},$$

where ε_{W} and ε_0 are the dielectric constants of water and free space, respectively, e is the elementary charge, N_{A} is Avogadro's number, k_{B} is Boltzmann's constant, T is the absolute temperature, and I is the ionic strength of the solution. As an example, for a particle interacting with the decane–water interface, the effective Hamaker constant is calculated from the combining relation (*i.e.*, $A_{\mathrm{eff}} = -6.94 \times 10^{-21}$ J), where the Hamaker constants of a polystyrene particle, water, and decane are $A_{\mathrm{P}} = 9.98 \times 10^{-20}$ J, $A_{\mathrm{W}} = 2.43 \times 10^{-20}$ J, and $A_{\mathrm{D}} = 3.97 \times 10^{-20}$ J, respectively.[36,37] The negative Hamaker constant leads to repulsive van der Waals interactions, and the magnitude of the interaction is negligibly small (*e.g.*, $\Pi_{\mathrm{vdW}} = O(-1)$ at h = 100 nm) compared to that of the double-layer interaction (*e.g.*, $\Pi_{\mathrm{el}} = O(2)$ at h = 100 nm).

The electrostatic double layer interaction is governed by the nonlinear PB equation

$$\frac{d^2\hat{\Psi}}{d\hat{h}^2} = \sinh\hat{\Psi}, \quad (1)$$

where $\hat{\Psi} = e\Psi/k_BT$ is the nondimensionalized potential of the planar surface. For planes with an identical charge and non-dimensional separation $\hat{h}_0 = \kappa h_0$, the boundary conditions are $\hat{\Psi} = \hat{\Psi}_0$ at $\hat{h} = 0$ and $\hat{\Psi}' = 0$ at the midpoint $\hat{h} = \hat{h}_0/2$ (due to symmetry). This nonlinear equation can be solved using either Jacobi elliptic functions[35,38] or numerical methods.[39,40] For example, the numerical solution can be obtained by substituting $\Psi_1 = \hat{\Psi}$ and $\Psi_2 = \hat{\Psi}'$:

$$\Psi_1' = \Psi_2$$
$$\Psi_2' = \sinh\Psi_1 \quad (2)$$

Here, the boundary conditions become $\Psi_1(0) = \hat{\Psi}_0$ and $\Psi_2(\hat{h}_0/2) = 0$ (the boundary value problem, BVP). Once the potential at the midplane $\hat{\Psi}_m = \hat{\Psi}(\hat{h}_0/2)$ is calculated, the nondimensionalized electrostatic disjoining pressure between the two planes can be obtained by

$$\hat{\Pi}_{el} = \frac{\Pi_{el}}{\gamma\kappa} = \frac{2n_0k_BT}{\gamma\kappa}\cosh\hat{\Psi}_m \quad (3)$$

Here, $n_0 = 1000N_AI$ is the number density of ions in solution.[41]

The numerical solution of the PB equation for two charged surfaces was also reported by Chan *et al.*[40] The potential $\hat{\Psi} = \Psi_1$ (eqn (2)) is integrated numerically from $\hat{h} = 0$, at which point, the potential is given by $\hat{\Psi} = \hat{\Psi}_m$, and the potential gradient becomes zero $d\hat{\Psi}/d\hat{h} = 0$ (the initial value problem, IVP). When the integrated potential reaches a given surface potential value $\hat{\Psi}_a$ at one surface plane, the corresponding distance of the plane from $\hat{h} = 0$ is determined to be $|\hat{h}_a|$. The same procedure is repeated to obtain the distance $|\hat{h}_b|$ for the other plane with $\hat{\Psi}_b$. The separation between the two planes is then $\hat{h} = |\hat{h}_a| + |\hat{h}_b|$, which is a function of $\hat{\Psi}_m$. Similarly, the electrostatic pressure between the two parallel planes is obtained by substituting the values of $\hat{\Psi}_m$ into eqn (3) (see the detailed method in the ESI†).

In general, the solution of the PB equation is approximated using both the Debye-Hückel approximation and the superposition approximation under conditions of low surface charge (*i.e.*, $|\Psi| < 50$ mV) and moderate overlap of the surface potentials (*i.e.*, $\Psi_m \approx \Psi_a(h_0/2) + \Psi_b(h_0/2)$ for $\kappa h \gg 1$).[36,41] Based on these assumptions, the analytical expression of the electrostatic disjoining pressure between two dissimilar parallel plane surfaces ($\hat{h} = 0$ and $\hat{h} = \hat{h}_0$) is found in a dimensionless form:[34]

$$\hat{\Pi}_{el} = \frac{\Pi_{el}}{\gamma\kappa} = -\frac{\kappa\varepsilon_0\varepsilon_W}{2\gamma\sinh\hat{h}}\left(\frac{\Psi_a^2 + \Psi_b^2}{\sinh\hat{h}} - 2\Psi_a\Psi_b\coth\hat{h}\right), \quad (4)$$

where Ψ_a and Ψ_b are the surface potentials.

The electrostatic double-layer interaction might be affected by the excluded volume of the hydrated electrolyte ions. Paunov and Binks found that the disjoining pressure increases with the finite size of ions for large separations (*i.e.*, superposition approximation for $\hat{h} = \kappa h \gg 1$).[42] The nondimensionalized analytical expression at fixed but identical surface potentials (*i.e.*, $\hat{\Psi} = \hat{\Psi}_a = \hat{\Psi}_b$) is

$$\hat{\Pi}_{el} = \frac{64n_0k_BT}{\gamma\kappa}\tanh^2\left(\frac{\hat{\psi}}{4}\right)\left[1 + 4\nu n_0\sinh^2\left(\frac{\hat{\psi}}{4}\right)\right]e^{-\hat{h}}, \quad (5)$$

where ν is the excluded volume parameter (*e.g.*, $\nu = 1.56 \times 10^{-27}$ m^3 for Na^+). At $\nu = 0$, eqn (5) can be reduced to[42]

$$\hat{\Pi}_{el} = \frac{64n_0k_BT}{\gamma\kappa}\tanh^2\left(\frac{\hat{\psi}}{4}\right)e^{-\hat{h}}, \quad (6)$$

where $\tanh^2(\hat{\Psi}/4) = \Upsilon_0$ is the Gouy–Chapman parameter.[41] Note that eqn (1)–(6) indicate the electrostatic interactions between two dissimilar parallel plane surfaces.

In order to estimate the electrostatic interaction force between a charged sphere and a charged non-deformable planar interface, the Derjaguin approximation can be used in the case of $\kappa a \gg 1$. Here, the sphere is approximated as a stack of infinitesimal circular rings with surface area dA_i.[41] The interaction force between the ith circular ring and the planar interface is

$$dF_{el,i} = \Pi_{el,i}dA_i. \quad (7)$$

From the geometrical relation, dA_i is replaced with $2\pi a d\xi$, where a is the radius of the sphere, and ξ is the distance between the ith circular ring and the interface. After substituting eqn (6) into eqn (7) (by replacing $\hat{h}$ with ξ) and integrating from $\xi = \hat{h}$ to $\xi =$ inf., the nondimensionalized interaction force for $\hat{h} \gg 1$ is

$$\hat{F}_{el} = \frac{\kappa F_{el}}{\gamma} = \frac{128\pi a n_0 k_BT}{\gamma}\tanh^2\hat{\psi}\,e^{-\hat{h}}. \quad (8)$$

Note that the upper limit $\xi =$ inf. for the integration is reasonable due to the exponential decay of the pressure with increasing distance.[41] Notably, if the radius of curvature of the interface deformation is sufficiently larger than the particle radius, eqn (7) and (8) can be applied for the deformable fluid–fluid interface.

Augmented Young–Laplace equation

The disjoining pressure between a fluid–fluid interface and a solid particle induces an interface deformation in which the normal components of the Maxwell stress tensors across the deformed interface are balanced by the normal components of the tensile stresses caused by surface tension.[34] When the particle size is sufficiently large compared to the Debye screening length ($\kappa a \gg 1$), the Derjaguin approximation can be used. This means that the disjoining pressure between the particle surface and an arbitrary location on the fluid interface is assumed to be identical to the pressure between planar surfaces with the same separation.[34] The augmented Young–Laplace equation estimates the shape of the interface deformation caused by the disjoining pressure as

$$\frac{\hat{z}''(\hat{r})}{(1 + \hat{z}'(\hat{r})^2)^{3/2}} + \frac{\hat{z}'(\hat{r})}{\hat{r}(1 + \hat{z}'(\hat{r})^2)^{1/2}} = \frac{\Delta\rho g\hat{z}(\hat{r})}{\gamma\kappa^2} - \hat{\Pi}(\hat{h}), \quad (9)$$

where the terms on the left-hand side of the equation are the radii of curvature, and the terms on the right-hand side indicate the nondimensionalized gravitational force and nondimensionalized disjoining pressure, respectively. In eqn (9), $\hat{r} = \kappa r$ is the dimensionless radial distance, $\Delta\rho$ is the density difference between the two fluids (in the case of decane and water, $\Delta\rho \approx 270$ kg m^{-3}), and g is the acceleration due to gravity. The nondimensionalized distance between the particle surface and the deformed interface $\hat{h}(\hat{r}) = \kappa h$ is related to the nondimensionalized height of the interface deformation $\hat{z}(\hat{r}) = \kappa z$ as $\hat{h} = \sqrt{(\hat{z} + \kappa a)^2 + \hat{r}^2} - \kappa a$ (see the geometry in Fig. 2). Initial conditions for eqn (9) are $\hat{z}'(\hat{r} \to 0) = 0$ and $\hat{z}(\hat{r} \to 0) = \hat{h}_0$.[29] The former condition represents symmetric deformation of the interface, and $\hat{h} = \kappa h_0$ in the latter condition is the dimensionless height of deformation above the particle center. In order to solve eqn (9), we set $z_1 = \hat{z}$ and $z_2 = \hat{z}'$, which lead to

$$z_1' = z_2$$
$$z_2' = \left[\frac{\Delta\rho g z_1}{\gamma\kappa^2} - \hat{\Pi}(\hat{h}) - \frac{z_2}{\hat{r}(1+z_2^2)^{1/2}}\right](1+z_2^2)^{3/2}, \quad (10)$$

where the two initial conditions are replaced with $z_1(\hat{r} \to 0) = \hat{h}_0$ and $z_2(\hat{r} \to 0) = 0$. Then, the interface profiles $\hat{z}(\hat{r})$ are numerically calculated by varying the value of $\hat{h}_0$.

Instantaneous but significant deformation can occur when the interface height, at a long distance from the particle, is smaller than the particle size. However, this is kinetically unstable[43–45] and often followed by the dewetting transition.[28,32] Therefore, we only account for the electrostatic double-layer interaction and the van der Waals interaction between the charged particles and a charged oil–water interface when calculating the interface deformation.[29,30,34,35]

Results and discussion

Disjoining pressure

We calculate the electrostatic disjoining pressure between two parallel planes with separation $\hat{h}$ using eqn (4) and (6), the BVP, and the IVP. For these calculations, the measured ξ-potential of the particles in the aqueous phase is approximately $\psi_{PW} \approx -80$ mV.[32] Marinova and coworkers measured the electrophoretic mobility of nonpolar oil droplets in the aqueous phase, in which the oil drop mobility depends weakly on the species of the oil and the ξ-potential plateaus at approximately $\psi_{DW} \approx -80$ mV, for an electrolyte concentration approaching infinite dilution.[46] The surface tension $\gamma \approx 50$ mN m^{-1} at the decane–water interface is measured using the pendant drop technique.[12] The ionic strength $I \approx 2.2 \times 10^{-6}$ M under normal atmospheric conditions corresponds to a Debye screening length of $\kappa^{-1} \approx 200$ nm.

As shown in Fig. 3a, the disjoining pressure obtained with eqn (6) is consistent with the both numerical solutions of BVP (eqn (2) and (3)) and IVP, even at small length scales ($\kappa h < 1$), compared to the result of eqn (4). Note that eqn (4) is based on the linearized PB equation with the assumptions of low surface charge ($|\psi| < 50$ mV) and large separation ($\kappa h \gg 1$).

Electrostatic interaction between a particle and an interface

The good agreement between the results from eqn (6) and the solutions of the nonlinear PB equations (BVP and IVP) shown in Fig. 3a rationalizes the expression of the double-layer force between a spherical particle and a planar interface (eqn (8)), which is derived from the Derjaguin approximation. As shown in Fig. 3b, the nondimensionalized double-layer interaction force, as calculated by eqn (8), exponentially decays with increased separation. For example, using parameter values of $\gamma \approx 50$ mN m^{-1} and $\kappa^{-1} \approx 200$ nm, the force between the particle and the oil–water interface is $F_{el} \approx 150$–250 pN at $h \approx 300$–200 nm.

In order to validate the scale of the obtained electrostatic force, we trap a particle in the aqueous subphase using optical tweezers and move the particle toward the oil–water interface. In most cases, the particle escapes from the optical trap before the dewetting transition occurs.[32,47] More quantitatively, assuming that the particle trapped in the aqueous phase escapes the optical trap at a half-radius of the particle ($\sim$0.7 μm, as an example),[48] we estimate the maximum trapping force $F_{trap}^{max} \approx 70$ pN at a calibrated laser power of $P_{63\times} \approx 150$ mW (when a water immersion objective (63× NA 1.2, Zeiss C-Apochromat) is used).[49–51] This value of F_{trap}^{max} is lower than the estimated electrostatic repulsion F_{el} at a certain separation distance between the particle and the oil–water interface. Consequently, the result demonstrates that the particle trapped by the laser tweezers should escape from the optical trap prior to the dewetting transition.[32]

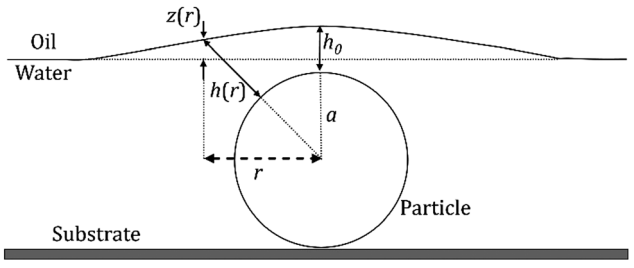

Fig. 2 Geometry of the interface deformation caused by the disjoining pressure.

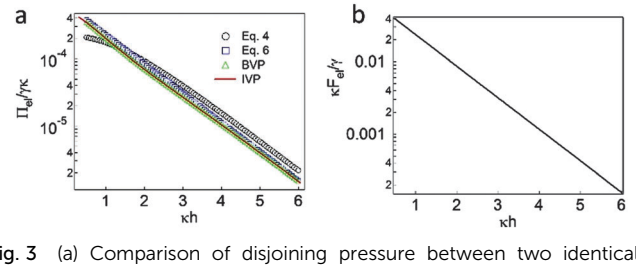

Fig. 3 (a) Comparison of disjoining pressure between two identically charged planes (*i.e.*, $\psi_{PW} = \psi_{DW} = -80$ mV) obtained using eqn (4) and (6), BVP, and IVP. (b) Nondimensionalized double-layer interaction force between a spherical particle and a planar interface (*i.e.*, $\psi_{PW} = \psi_{DW} = -80$ mV), as obtained from eqn (8).

Augmented Young–Laplace equation: interface deformation

The augmented Young–Laplace equation (eqn (10)) is numerically solved to obtain the curved interface profiles. We use eqn (6) as an analytical expression of the disjoining pressure in eqn (10). As shown in Fig. 4a, the resulting interface deformation (solid lines) is indicated as a function of the nondimensionalized radial distance κr and the nondimensionalized initial height of the interface (κh_0). The dashed line indicates a portion of the particle surface (*e.g.*, at $\kappa h_0 = 0.5$). The interface deformation becomes significant as the interface is lowered due to the disjoining pressure, which decays exponentially upon separation (eqn (6)). Note that the interface deformation is on the order of a few nanometers at a Debye length of $\kappa^{-1} \approx 200$ nm, which is consistent with other values reported in the literature.[29,30]

Lateral capillary interactions

It is assumed that assembly occurs at equilibrium (*i.e.*, a fixed interface height at a certain moment). This is a reasonable assumption because the mean separation between particles in the assembled crystal structure slowly decreases with time (*i.e.*, $\sim 2.2 \times 10^{-2}$ nm s^{-1}) after the assembly is formed.[32] Therefore, we do not consider the dribble of particles caused by lateral movement of the slant interface[52] or the crystal hardening caused by thin-film drainage.[43–45] The DLVO interactions (*i.e.*, electrostatic double-layer interaction and van der Waals interaction) between the particles immersed in the aqueous phase are negligible compared to the lateral capillary attractions.[17]

Assuming that the interface deformation above the particles occurs symmetrically with respect to the center of the particles, the lateral capillary interaction between two neighboring particles with separation L can be expressed as $\Phi_{cap}(L) = \Delta G = G - G_0$.[16,39,50] $G = 2\gamma(s_D' - s_0')$ and $G_0 = 2\gamma(s_D - s_0)$ indicate the surface free energy when the deformed interfaces above the two particles are overlapped and not overlapped with each other, respectively. Additionally, s_D and s_0 denote the deformed interface area and the corresponding projected area on a flat surface, respectively, which can be obtained by numerically integrating the infinitesimal surface area. As shown in Fig. 4b, the resulting capillary force between two particles beneath the deformed oil–water interface increases as the interface height κh_0 decreases. The enhanced capillary force between the particles suggests that the resulting colloidal crystal becomes stiffer as the interface height decreases; this is consistent with the experimental observations.[32] Notably, it is found that the capillary force decays as $F_{cap} \sim 1/L$, which is a hallmark of capillary forces caused by symmetric and monopolar interface deformation.[17]

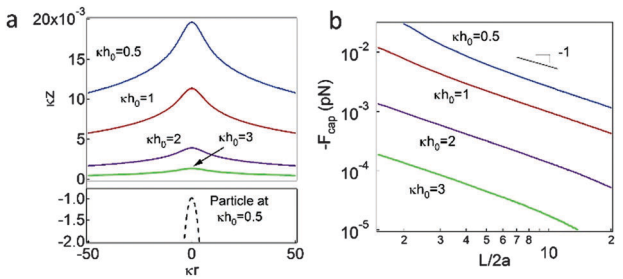

Fig. 4 (a) Dimensionless interface profiles obtained by solving the augmented Young–Laplace equation (eqn (6) and (10)). The solid lines represent the curved interfaces with various initial heights of the interface κh_0. The dashed line represents the particle surface at $\kappa h_0 = 0.50$. (b) Lateral capillary forces F_{cap} between two particles.

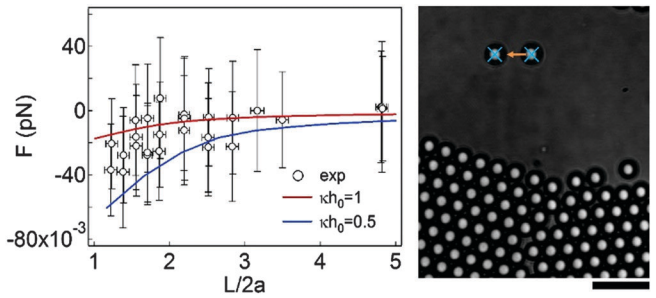

Fig. 5 Comparison of the calculations and the direction measurement of the pair interaction force using optical tweezers. The maximum trapping force for the pair interaction measurement is $F_{trap}^{max} \approx 0.8$ pN at a calibrated laser power $P_{63\times} \approx 2.6$ mW.[49] The microscopic image on the right-hand side is extracted from Movie S2 in the ESI.† The scale bar is 10 μm.

To verify our calculations, we disturb the structure of the assembled crystal by holding two particles and translating one of them with optical laser tweezers at $F_{trap}^{max} \approx 70$ pN (Movie S1 in the ESI†). The fact that the assembly structure can be disturbed by the optical traps demonstrates that the modulus of crystal rigidity is on the scale of tens of piconewtons. For a more quantitative measurement, we trap two particles in the assembly using the optical tweezers and transfer them to a particle-absent region. In order to measure the pair interaction force between the two trapped particles, the right-most particle in Fig. 5 approaches the stationary particle that is displaced (Δx) from its equilibrium position, depending on the magnitude of attraction (see Movie S2 in the ESI†).[2,14,15,21] The interaction force is then calculated by $F = \kappa_t \Delta x$ where κ_t is a calibrated trap stiffness and is related to the particle separation (L). As shown in Fig. 5, the scale of the measured interaction force is consistent with the calculated results when the value of κh_0 is between 0.5 and 1.0. Therefore, the assembly behaviors of the colloidal crystals confined between the oil–water interface and the solid substrate can be attributed to the electrostatic disjoining pressure between the particles and the interface, which consequently leads to interface deformation and lateral capillary attraction.

Conclusions

We reported the lateral capillary interaction of colloidal particles that stems from the out-of-plane electrostatic disjoining pressure between charged particles and a charged interface. The symmetric interface deformation above the particles, which is caused by the electrostatic disjoining pressure, generates the capillary force that leads to the formation of a closely packed assembled crystal. Based on our numerical calculations, the estimated capillary force decays as $F_{cap} \sim 1/L$, which is a hallmark of capillary forces caused by symmetric and monopolar interface deformation. Interestingly,

it is notable that the short-range double-layer repulsive interactions (*i.e.*, on the nanometer scale) can generate long-range lateral capillary attractions (*i.e.*, on the micrometer scale). The capillary interaction model in this work accounts for the unique properties of the particle assembly, including the crystal reversibility against structural disturbance *via* optical laser tweezers (Movie S1 in ESI†) and the ability to control the rigidity of the crystal by manipulating the interface height.[32]

Acknowledgements

This work was supported by the Engineering Research Center of Excellence Program of the Korea Ministry of Science, ICT & Future Planning (MSIP)/National Research Foundation of Korea (NRF) (NRF-2014R1A5A1009799).

Notes and references

1 J. A. Weiss, A. E. Larsen and D. G. Grier, *J. Chem. Phys.*, 1998, **109**, 8659–8666.
2 J. P. Pantina and E. M. Furst, *Langmuir*, 2004, **20**, 3940–3946.
3 A. E. Larsen and D. G. Grier, *Nature*, 1997, **385**, 230–233.
4 M. E. Leunissen, A. Van Blaaderen, A. D. Hollingsworth, M. T. Sullivan and P. M. Chaikin, *Proc. Natl. Acad. Sci. U. S. A.*, 2007, **104**, 2585–2590.
5 F. Oosawa and S. Asakura, *J. Chem. Phys.*, 1954, **22**, 1255.
6 J. P. Pantina and E. M. Furst, *Phys. Rev. Lett.*, 2005, **94**, 138301.
7 B. P. Binks and T. S. Horozov, *Colloidal Particles at Liquid Interfaces*, Cambridge University Press, New York, 2006.
8 B. J. Park, D. Lee and E. M. Furst, *Particle-Stabilized Emulsions and Colloids: Formation and Applications*, The Royal Society of Chemistry, 2015, pp. 8–44.
9 B. J. Park and D. Lee, *MRS Bull.*, 2014, **39**, 1089–1098.
10 P. Pieranski, *Phys. Rev. Lett.*, 1980, **45**, 569–572.
11 A. J. Hurd, *J. Phys. A: Math. Gen.*, 1985, **45**, L1055–L1060.
12 S. Reynaert, P. Moldenaers and J. Vermant, *Langmuir*, 2006, **22**, 4936–4945.
13 M. Oettel and S. Dietrich, *Langmuir*, 2008, **24**, 1425.
14 B. J. Park, J. P. Pantina, E. M. Furst, M. Oettel, S. Reynaert and J. Vermant, *Langmuir*, 2008, **24**, 1686–1694.
15 B. J. Park, J. Vermant and E. M. Furst, *Soft Matter*, 2010, **6**, 5327–5333.
16 K. Masschaele, B. J. Park, E. M. Furst, J. Fransaer and J. Vermant, *Phys. Rev. Lett.*, 2010, **105**, 048303.
17 P. A. Kralchevsky and K. Nagayama, *Langmuir*, 1994, **10**, 23–36.
18 D. Stamou, C. Duschl and D. Johannsmann, *Phys. Rev. E: Stat. Phys., Plasmas, Fluids, Relat. Interdiscip. Top.*, 2000, **62**, 5263–5272.
19 M. Oettel, A. Dominguez and S. Dietrich, *Phys. Rev. E: Stat., Nonlinear, Soft Matter Phys.*, 2005, **71**, 051401.
20 E. J. Stancik, M. J. O. Widenbrant, A. T. Laschitsch, J. Vermant and G. G. Fuller, *Langmuir*, 2002, **18**, 4372–4375.
21 B. J. Park and E. M. Furst, *Soft Matter*, 2011, **7**, 7676–7682.
22 B. J. Park and E. M. Furst, *Soft Matter*, 2011, **7**, 7683–7688.
23 K. Masschaele, J. Fransaer and J. Vermant, *Soft Matter*, 2011, **7**, 7717–7726.
24 S. U. Pickering, *J. Chem. Soc., Trans.*, 1907, **91**, 2001–2021.
25 A. D. Dinsmore, M. F. Hsu, M. G. Nikolaides, M. Marquez, A. R. Bausch and D. A. Weitz, *Science*, 2002, **298**, 1006–1009.
26 E. M. Herzig, K. A. White, A. B. Schofield, W. C. K. Poon and P. S. Clegg, *Nat. Mater.*, 2007, **6**, 966–971.
27 S. V. Jan Vermant, C. Dewitte and P. Moldenaers, *Rheol. Acta*, 2008, **47**, 835–839.
28 B. P. Binks, *Curr. Opin. Colloid Interface Sci.*, 2002, **7**, 21–41.
29 D. Bhatt, J. Newman and C. J. Radke, *J. Phys. Chem. B*, 2003, **107**, 13076–13083.
30 D. E. Aston and J. C. Berg, *J. Colloid Interface Sci.*, 2001, **235**, 162–169.
31 D. Y. C. Chan, R. R. Dagastine and L. R. White, *J. Colloid Interface Sci.*, 2001, **236**, 141–154.
32 B. J. Park and E. M. Furst, *Soft Matter*, 2010, **6**, 485–488.
33 N. D. Denkov, O. D. Velev, P. A. Kralchevsky, I. B. Ivanov, H. Yoshimura and K. Nagayama, *Nature*, 1993, **361**, 26.
34 D. J. Bachmann and S. J. Miklavcic, *Langmuir*, 1996, **12**, 4197–4204.
35 S. J. Miklavcic, *Phys. Rev. E: Stat. Phys., Plasmas, Fluids, Relat. Interdiscip. Top.*, 1996, **54**, 6551–6556.
36 J. N. Israelachvili, *Intermolecular and Surface Forces*, Academic Press, New York, 3rd edn, 2011.
37 C. M. Roth and A. M. Lenhoff, *J. Colloid Interface Sci.*, 1996, **179**, 637–639.
38 D. McCormack, S. L. Carnie and D. Y. C. Chan, *J. Colloid Interface Sci.*, 1995, **169**, 177–196.
39 J. N. Connor and R. G. Horn, *Langmuir*, 2001, **17**, 7194–7197.
40 D. Y. C. Chan, R. M. Pashley and L. R. White, *J. Colloid Interface Sci.*, 1980, **77**, 283–285.
41 P. C. Hiemenz and R. Rajagopalan, *Principles of Colloid and Surface Chemistry, revised and expanded*, CRC press, 1997.
42 V. N. Paunov and B. P. Binks, *Langmuir*, 1999, **15**, 2015–2021.
43 L. G. Cascão Pereira, C. Johansson, C. J. Radke and H. W. Blanch, *Langmuir*, 2003, **19**, 7503–7513.
44 K. Kumar, A. D. Nikolov and D. T. Wasan, *J. Colloid Interface Sci.*, 2002, **256**, 194–200.
45 I. Ivanov, *Thin liquid films*, CRC Press, 1988.
46 K. G. Marinova, R. G. Alargova, N. D. Denkov, O. D. Velev, D. N. Petsev, I. B. Ivanov and R. P. Borwankar, *Langmuir*, 1996, **12**, 2045–2051.
47 B. J. Park, *Korean Chem. Eng. Res.*, 2013, **51**, 527–530.
48 R. M. Simmons, J. T. Finer, S. Chu and J. A. Spudich, *Biophys. J.*, 1996, **70**, 1813–1822.
49 B. J. Park and E. M. Furst, *Langmuir*, 2008, **24**, 13383–13392.
50 B. J. Park and E. M. Furst, *Macromol. Res.*, 2013, **11**, 1167–1170.
51 B. J. Park and E. M. Furst, *Langmuir*, 2014, **30**, 11055–11061.
52 J. Sur and H. K. Pak, *Phys. Rev. Lett.*, 2001, **86**, 4326–4329.